Spline-Kernelled Chirplet Transform for the Analysis of Signals With Time-Varying Frequency and Its Application

Y. Yang, Z. K. Peng, G. Meng, and W. M. Zhang

***Abstract*—The conventional time–frequency analysis (TFA) methods, including continuous wavelet transform, short-time Fourier transform, and Wigner–Ville distribution, have played important roles in analyzing nonstationary signals. However, they often show less capability in dealing with nonstationary signals with time-varying frequency due to the bad energy concentration in the time–frequency plane. On the other hand, by introducing an extra transform kernel that matches the instantaneous frequency of the signal, parameterized TFA methods show powerful ability in characterizing time–frequency patterns of nonstationary signals with time-varying frequency. In this paper, a novel time–frequency transform, called spline-kernelled chirplet transform (SCT), is proposed. By introducing a frequency-rotate operator and a frequency-shift operator constructed with spline kernel function, the SCT is particularly powerful for the strongly nonlinear frequency-modulated signals. In addition, an effective algorithm is developed to estimate the parameters of transform kernel in the SCT. The capabilities of the SCT and parameter estimation algorithm are validated by their applications for numerical signals and a set of vibration signal collected from a rotor test rig.**

***Index Terms*—Chirplet transform (CT), instantaneous frequency (IF), spline-kernelled chirplet transform (SCT), time–frequency representation (TFR).**

I. Introduction

INSTANTANEOUS FREQUENCY (IF) [1], [2], as an informative time–frequency characteristic of a signal, plays an important role in nonstationary signal analysis. Estimation of the IF is desirable in the fields of rotary machine [3]–[8], power system [9], [10], electronic system [11], speech [12], wind turbine [13], transportation system [14], and others, where the IFs are often used to characterize important physical parameters of the signals. To estimate the IF, time–frequency analysis (TFA) methods [15], [16] are often applied, and the estimation accuracy usually depends on the energy concentration of the time–frequency representation (TFR) produced by TFA methods.

Manuscript received March 18, 2011; revised June 27, 2011; accepted July 8, 2011. Date of publication August 4, 2011; date of current version October 25, 2011. This work was supported in part by the National Natural Science Foundation of China under Grants 10902068 and 10732060 and in part by Shanghai Pujiang Program under Grant 10PJ1406000.

The authors are with the State Key Laboratory of Mechanical System and Vibration, Shanghai Jiao Tong University, Shanghai, 200240, China (e-mail: emma002@sjtu.edu.cn; pengzhike@tsinghua.org.cn; gmeng@sjtu.edu.cn; wenmingz@sjtu.edu.cn).

Color versions of one or more of the figures in this paper are available online at http://ieeexplore.ieee.org.

Digital Object Identifier 10.1109/TIE.2011.2163376

Among a number of TFA methods, short-time Fourier transform (STFT) [17]–[19], wavelet transform (WT) [10], [20], and Wigner–Ville distribution (WVD) [3], [5], [5] have been widely used; they are nonparameterized methods [21]. For the STFT method, the signal is assumed to be piecewise stationary at the scale of the window width as the STFT relies on traditional Fourier transform, and therefore, the STFT cannot produce an accurate estimation for time-varying IFs. Essentially, the WT is a kind of STFT method with adjustable window size, using large window for low-frequency components and small window for high-frequency components. Thus, it is no wonder that the WT cannot achieve an accurate estimation for time-varying IFs as well [22]. The WVD can present excellent TFR for signals in terms of energy concentration, but its bilinear structure creates the redundant cross terms that do not indicate the true time–frequency structure of the signal, which leads to inaccurate estimation of IFs.

In order to capture the accurate time–frequency pattern of chirplike signal, chirplet transform (CT), a parameterized time–frequency transform, has been developed, and now, it has been often used in the analysis of linear-frequency-modulated (LFM) signals [23], [24]. Compared with STFT, CT possesses an extra chirp kernel, which is characterized by a chirping rate parameter. With the transform kernel, the time–frequency atoms of the CT can be shifted and sheared to suit the signal. Nonetheless, the CT fails to characterize the underlying time–frequency pattern of nonlinear-frequency-modulated (NLFM) signals as it is impossible for the chirp kernel to match the nonlinear IF of NLFM signal. To overcome the shortcoming of the CT, Chassande-Mottin and Pai [25] developed a general chirplet chain (CC) method to analyze gravitational wave signals with nonlinearly time-varying IFs. By maximizing an optimal statistics, the method is used to find the best CC whose IF is essentially a piecewise linear approximation of the IF to be detected. Mihovilovic and Bracewell [26] proposed an adaptive CT to improve the TFR so as to estimate IF for NLFM signals. With a frequency drift rate, this method is able to adjust the tilt angle of time–frequency atom to match the NLFM signals in the time–frequency plane. The local frequency drift rate can be estimated by the slope of the line which approximates the energy ridge locally in the TFR. Cui and Wong [27] proposed another adaptive CT based on matching pursuit method and applied it to characterize the time-dependent behavior of the visual evoked potential from its initial transient portion to the steady-state portion. In their study, the signal is assumed to

be a sum of a series of weighted chirplets and residue, and the method iteratively projects the residue of the signal into a predefined chirplet dictionary. The best-matched chirplets can be determined by maximizing a similarity degree. In the essence, the aims of these "adaptive" CTs are to find the best-fit straight lines with arbitrary slopes to approximate the signal's energy ridge locally in the time–frequency plane. However, it is obvious that the broken line is neither very smooth nor very accurate approximation for highly nonlinear curve. Moreover, the boundary effect of decomposed chirplets in the TFR can mislead the identification and extraction of the IF.

In this paper, a novel time–frequency transform, named as spline-kernelled CT (SCT), is proposed based on the conventional CT. By implementing a frequency-rotate operator and a frequency-shift operator constructed with spline kernel, it is able to characterize the underlying time–frequency pattern of the signal with nonlinearly time-varying IF as it can be well approximated by a spline function. Moreover, the parameters of the spline kernel of the SCT can be estimated through the spline approximation. Therefore, the SCT is able to produce a TFR with an excellent energy concentration for signal with nonlinearly time-varying IF so as to facilitate the accurate IF estimation. The rest of this paper is organized as follows. Section II briefly introduces the conventional CT, the spline function, and the underlying principle of the SCT. In Section III, the parameter estimation algorithm for the SCT is presented. A signal contaminated by the noise is used to demonstrate the effectiveness of the proposed algorithm. Section IV evaluates the proposed SCT algorithm on several numerical examples and a set of signals collected from a rotor test rig. The conclusions are drawn in Section V.

II. SCT

In this section, the detail of the SCT is described after a brief introduction of the CT and the spline function.

A. CT

CT is basically the inner product of the signal to be analyzed and a family of analysis windows. For a frequency-modulated signal $s(t) \in \mathbf{L}^2(R)$, its CT at τ is defined as [28]

$$CT(\tau,\omega,\alpha;\sigma) = \int_{-\infty}^{+\infty} z(t)\exp\left[-j\frac{\alpha}{2}(t-\tau)^2\right] w_\sigma(t-\tau) \times \exp(-j\omega t)dt \quad (1)$$

where τ and $\alpha \in R$ stand for time and chirping rate, respectively. $z(t)$ is the analytical signal of $s(t)$, calculated by a Hilbert transform [29] $\boldsymbol{H}$, i.e., $z(t) = s(t) + j\boldsymbol{H}[s(t)]$. Since the Hilbert transform is only very effective for the high sampling rate [30], the sampling rate should be set appropriately in order to obtain the correct analytical signal. $w_\sigma(t)$ is a nonnegative, symmetric, and normalized real window, which is often taken as the Gaussian window function defined as

$$w_\sigma(t) = \frac{1}{\sqrt{2\pi}\sigma}\exp\left(-\frac{1}{2}\left(\frac{t}{\sigma}\right)^2\right). \quad (2)$$

According to definition (1), the CT of a signal is equivalent to the STFT of its analytical signal multiplied by the complex window $\psi(t,\alpha)$. The CT can also be rewritten as

$$CT(\tau,\omega,\alpha;\sigma) = A\int_{-\infty}^{\infty} \bar{z}(t)w_\sigma(t-\tau)\exp(-j\omega t)dt \quad (3)$$

with

$$\begin{aligned}\bar{z}(t) &= z(t)\Phi^R(t,\alpha)\Phi^S(t,\tau,\alpha)\\ \Phi^R(t,\alpha) &= \exp(-j\alpha t^2/2)\\ \Phi^S(t,\tau,\alpha) &= \exp(j\alpha\tau t)\\ A(\tau,\alpha) &= \exp(-j\tau^2\alpha/2)\end{aligned}$$

where $A(\tau,\alpha)$ is a complex value with modulus $|A(\tau,\alpha)| = 1$. In the time–frequency analysis, it is the modulus of the TFR, $|CT(\tau,\omega,\alpha;\sigma)|$, that is usually of interests and meaningful, so the CT can be simplified as

$$CT(\tau,\omega,\alpha;\sigma) = \int_{-\infty}^{\infty} \bar{z}(t)w_\sigma(t-\tau)\exp(-j\omega t)dt \quad (4)$$

where $\Phi^R(t,\alpha)$ and $\Phi^S(t,\tau,\alpha)$ are named as the frequency-rotate operator and the frequency-shift operator, respectively. To elaborate the functionality of these two operators, an LFM signal is considered, i.e.,

$$s(t) = \sin(2\pi\omega_0 t + \pi\lambda t^2). \quad (5)$$

The IF of the signal is $\Omega(t) = \omega_0 + \lambda t$, where λ is the slope of the IF trajectory and ω_0 is the initial frequency. In the CT of $s(t)$, $\Phi^R(t,\alpha)$ rotates the analytical signal $z(t)$ by an angle $\arctan(-\alpha)$ in the time–frequency plane. If the chirping rate α equals λ, then the frequency of the analytical signal is equivalent to ω_0 all the time, and then, $\Phi^S(t,\tau,\alpha)$ relocates the frequency component of the signal at time τ with an increment of $\alpha\tau$. It is noticed that the frequency of $z(t)$ at time τ after CT would be equal $\Omega(\tau)$ when $\alpha = \lambda$. Therefore, the CT can be essentially decomposed into a series of operations: First, the signal is rotated by a degree $\arctan(-\alpha)$ in the time–frequency plane. Second, it is shifted by a frequency increment of $\alpha\tau$ in the time–frequency plane. Next, it is processed by the STFT with the window w_σ.

It is worth noticing that the frequency resolution of the CT depends on the chirping rate α and the length of the Gaussian window. Taking the signal denoted in (5) as an example, the time–frequency atom adopted by the CT is of bandwidth of $\sigma|\lambda-\alpha| + 1/\sigma$ and duration of σ to divide the time–frequency plane. When $\alpha = \lambda$, the time–frequency atom has a minimum bandwidth of $1/\sigma$ and a duration of σ, which is the same as that of the Gaussian window. Obviously, the CT degrades to STFT when $\alpha = 0$. Given the proper chirping rate, the CT can produce a TFR with an optimal energy concentration, and $|CT(\tau,\omega,\alpha;\sigma)|$ achieves global maximum at $(\omega,\alpha) = (\omega_0,\lambda)$.

B. Spline Function

It seems reasonable for the adaptive CT to calculate the approximation when the straight line can accurately fit the IF in a properly determined interval. However, the obvious disadvantage of the broken line approximation lies in its lack of smoothness as well as its excessive computational load for interval determination. According to Weierstrass approximation theorem [31], polynomial is a better choice to provide smoother and more efficient approximation to continuous function than the broken lines. However, polynomial approximation is not necessarily good. The Gram matrix would be ill-conditioned in solving the least square approximation with a polynomial of high order, which is worse as the order of polynomial increase. Moreover, if a function is to be approximated on a larger interval, the order of the approximating polynomial has to be chosen unacceptably large. Thus, it will be difficult to compute the least square polynomial when the Gram matrix is highly ill-conditioned, which leads to inaccurate approximation for the data to be matched.

Spline is known to be effective in approximating high dynamic shapes on a larger interval. It can be defined as a piecewise polynomial function with boundary constraints at jointed breaks. The broken line is the spline of order 2. On an interval $[a, b]$ with breaks $a = t_1 < \cdots < t_{l+1} = b$, a spline of order n can be defined in piecewise polynomial form (ppform) with l pieces as [33]

$$S(x) = P_i(x), \quad \text{for} \quad x \in (t_i, t_{i+1}) \tag{6}$$

with $P_i(x) = \sum_{k=1}^{n} p_k^i (x - t_i)^{k-1}$ for $i = 1, \ldots, l$ where p_k^i denotes the local polynomial coefficients. Two consecutive polynomials are required to share the same $n-2$ derivatives at the breaks to be jointed, i.e., $P_i^{(d)}(t_i) = P_{i+1}^{(d)}(t_i)$, where $0 \le d \le n-2$. In this paper, the breaks are uniformly placed if there is no special instruction.

As stated in Section II-A, the frequency-rotate operator of the CT is essentially an exponential function of the integral of the linear function characterized by chirping rate. Accordingly, the indefinite integral of the local polynomial defined in (6) is derived as

$$\int P_i(x)dx = \sum_{k=1}^{n} \frac{p_k^i}{k}(x - t_i)^k + o_i \tag{7}$$

where o_i is the integral constant of the local polynomial. The ppform composed by (7) with boundary constraints can be a spline of $n+1$ order. In order to hold the continuous $n-2$ derivatives at the jointed breaks, the integral constant o_i is demanded to satisfy the constraint as follows:

$$o_i - o_{i+1} = \sum_{k=1}^{n} \frac{p_k^{i+1}}{k}(t_i - t_{i+1})^k. \tag{8}$$

Given the piecewise nature of spline, it is able to approximate the discontinuous function by loosening the restrictions at the specific breaks. For example, the function to be approximated is discontinuous at t_i, and the continuity requirements of the approximated spline at this break are broken so that $P_i^{(d)}(t_i) \neq P_{i+1}^{(d)}(t_i)$. It is equivalent to divide a spline into two subspline segments, and each one of them is a separate spline.

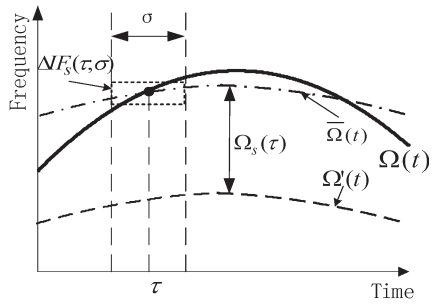

Fig. 1. Illustration of SCT principal. (Solid line) IF of signal. (Dashed line) IF trajectory after rotation. (Dotted line) IF trajectory after rotation and shift.

C. SCT

In order to characterize the time–frequency patterns of signals with nonlinearly time-varying frequency, the SCT is proposed. By replacing the kernel of the frequency-rotate operator and frequency-shift operator in the conventional CT with a spline kernel, the proposed SCT extends the capability of the conventional CT and can be applied to a wider class of signals, i.e., the NLFM signals whose IF trajectory can be approximated by a spline function as in (9). The SCT of a signal is defined as

$$SCT(\tau, \omega, Q; \sigma) = \int_{-\infty}^{+\infty} \bar{z}(t) w_\sigma(t - \tau) \exp(-j\omega t) dt \quad \text{for} \quad \tau \in (t_i, t_{i+1}) \tag{9}$$

with

$$\bar{z}(t) = z(t)\Phi^R(t, Q)\Phi^S(t, \tau, Q)$$
$$\Phi^R(t, Q) = \exp\left(-j\sum_{k=1}^{n} \frac{q_k^i}{k}(t - t_i)^k + \gamma_i\right)$$
$$\Phi^S(t, \tau, Q) = \exp\left(j\sum_{k=1}^{n} q_k^i(\tau - t_i)^{k-1} t\right)$$

where $\Phi^R(t, Q)$ and $\Phi^S(t, \tau, Q)$ are frequency-rotate operator and frequency-shift operator, respectively; $Q(i, k) = q_k^i$ denotes the local polynomial coefficient matrix of the spline kernel; and γ_i is required to satisfy

$$\gamma_i - \gamma_{i+1} = \sum_{k=1}^{n} \frac{q_k^{i+1}}{k}(t_i - t_{i+1})^k \tag{10}$$

with $\gamma_1 = 0$.

Specifically, the SCT includes three sequential operations: 1) the signal is rotated in the time–frequency plane by adding the IF of $\Phi^R(t, Q)$, i.e., $\Omega_R(t) = -\sum_{k=1}^{n} q_k^i (t - t_i)^{k-1}$; 2) the signal is shifted in the time–frequency plane by adding the frequency of $\Phi^S(t, \tau, Q)$ at τ, i.e., $\Omega_s(\tau) = \sum_{k=1}^{n} q_k^i (\tau - t_i)^{k-1}$; and 3) the signal is processed by the STFT with window w_σ.

Fig. 1 shows the principal of the SCT, where $\Omega(t)$, $\Omega'(t)$, and $\bar{\Omega}(t)$ represent the true IF of the signal, the rotated IF, and the eventual obtained IF of the signal by the SCT, respectively. Denote the range of $\Omega(t) + \Omega_R(t)$ at the time span $[\tau - \sigma/2, \tau + \sigma/2]$ as $\Delta IF_s(\tau; \sigma)$. The frequency resolution of

the SCT is determined by both $\Delta IF_s(\tau;\sigma)$ and the bandwidth of the Gaussian function $1/\sigma$, i.e., the frequency resolution at τ equals $\Delta IF_s(\tau;\sigma)+1/\sigma$. If q_k^i is well selected to equal p_k^i, for all i and k, $\Delta IF_s(\tau;\sigma)$ will become zero all over the time span, and the frequency resolutions of the SCT at any moments can reach the minimum $1/\sigma$.

III. Parameter Estimation Method

It is crucial to develop a parameter estimation method for the SCT to facilitate the construction of the spline kernel function that can approximate the IF of the signal in real applications. Only with the appropriately determined parameters can SCT attain a satisfactory TFR with an excellent concentration and achieve the IF estimation with significant accuracy. The spline approximation is introduced to estimate the parameters of the transform kernel of the SCT. According to [33], any spline function of a given degree and smoothness can be represented as a weighted sum of basic splines (b-splines). As another way to represent a spline, B-form has become a standard representation other than the ppform for its convenience of constructing and shaping a function, which is defined as

$$S(x)=\sum_{j=1}^{m} c_j B_{j,n}(x) \quad \text{for} \quad a\le x\le b \tag{11}$$

where m is the number of the b-splines and c_j is the control point. $B_{j,n}$ denotes the jth b-spline of order n for a knot sequence, i.e., $v_1\le v_2\ldots\le v_{m+n}$. It should be noted that the knots are different from the aforementioned breaks in that they are repeated. Simply, apart from the interior breaks, the knot sequence should contain the two endpoints, a and b, of the basic interval exactly n times. Thus, breaks can be the interior breaks of knot sequence, which may be repeated depending on the required constraints. In particular, $B_{j,n}$ is nonnegative piecewise polynomial with breaks $v_j,\ldots,v_{j+n}$ and is zero outside the interval $(v_j,\ldots,v_{j+n})$, which can be computed as

$$B_{j,1}(x)=\begin{cases}1 & \text{if } v_j\le x<v_{j+1}\\ 0 & \text{otherwise}\end{cases} \tag{12}$$

$$B_{j,n}(x)=\frac{x-v_j}{v_{j+n-1}-v_j}B_{j,n-1}(x)+\frac{v_{j+n}-x}{v_{j+n}-v_{j+1}}B_{j+1,n-1}(x). \tag{13}$$

To obtain a smoothing spline that can approximate a set of noisy data $(x_i,y_i)_1^N$ for $x_i\in[a,b]$, it is required to minimize

$$\sum_i w_i\left(y_i-S(x_i)\right)^2+\lambda\int_a^b\left(S^{(d)}(v)\right)^2 dv \tag{14}$$

with given positive weights w_i and smoothing parameter λ. Unser *et al.* [34], [35] provided an efficient solution to (14) and obtained a matched spline in B-form. Since the ppform and the B-form are essentially the different representations for the same spline, the two forms can be converted to each other. The B-form of the spline can be converted to its local power form by applying Taylor expansion at the left beginning of each nonzero knot span with the appropriate number of terms depending on the required degree [36]. In addition, to determine whether there are intermittent points or not, the Euclidean distance between the successive data points, denoted by $D(x_i)$, for $i=1:N-1$, can be measured. As long as $D(x_o)>\Delta$, in which Δ is the threshold, the intermittent point of (x_o,y_o) is determined as an interior break. In this case, the constraint at (x_o,y_o) needs to be loosened, and thus the spline kernel is broken into separate segments.

An iterative procedure based on the TFR is proposed to estimate the parameters from the unknown signal with nonlinearly time-varying frequency. At first, the TFR is obtained by using the SCT with initialized parameter matrix $q(i,k)=q_k^i=0$, for all i and k, which makes SCT degrade to STFT. Since the energy of a signal is mainly distributed around the IF of the signal in the time–frequency plane, the IF can be estimated through the time–frequency peak detection. The position of the energy peak in the TFR is denoted as the estimated IF of the considered signal

$$\widetilde{\Omega}(t)=\arg\max_{\omega}\left(|SCT(t,\omega,Q;\sigma)|\right). \tag{15}$$

Second, a spline function is selected to approximate $\widetilde{\Omega}(t)$ by solving (14). Once the best fitted spline is calculated, a proper frequency-rotate operator and frequency-shift operator of the SCT can be constructed for the SCT. Next, using the estimated parameters, the SCT generates an improved TFR with a better energy concentration. This procedure keeps iterating until no more evident modification is observed in the estimated IF, i.e.,

$$\zeta_{\text{iter}}=mean\int\frac{\left|\widetilde{\Omega}_{\text{iter}+1}(t)-\widetilde{\Omega}_{\text{iter}}(t)\right|}{\left|\widetilde{\Omega}_{\text{iter}}(t)\right|}dt<\delta \tag{16}$$

where δ is a predetermined threshold and the subscript denotes the index of the iteration. The detail of the algorithm is described as follows.

Initialization:

Initialized parameter matrix, Q, number of spline pieces, minor integer δ, window size, maximum iteration $L_{\max}$, threshold Δ.

Output: parameters of the estimated IF

While $iter<L_{\max}$ and $\zeta_{\text{iter}}<\delta$

1) Generating TFR for $s(t)$ by using SCT with Q.
2) Extracting $\widetilde{\Omega}_{\text{iter}}(t)$ according to (15) in obtained TFR.
3) Calculating $D(t)$ for $\widetilde{\Omega}_{\text{iter}}(t)$
4) **If** $D(t_o)>\Delta$, **then**
   1) Finding subspline for each segment of $\widetilde{\Omega}_{\text{iter}}(t)$ by solving (14);
   2) Combining all the segments.

   Else then

   Finding a spline to approximate $\widetilde{\Omega}_{iter}(t)$ by solving (14)
5) Obtaining new parameter matrix $\overline{Q}$.
6) Updating Q with $\overline{Q}$.
7) Calculating ζ_{iter} according to (16) and let $iter\leftarrow iter+1$

End

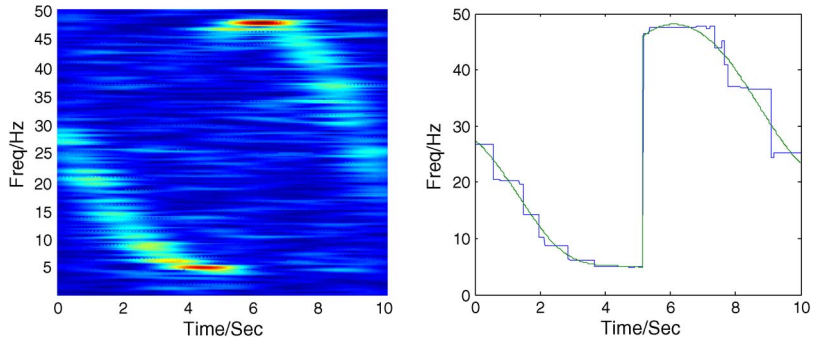

Fig. 2. SCT-based TFR and estimated IF in the first iteration.

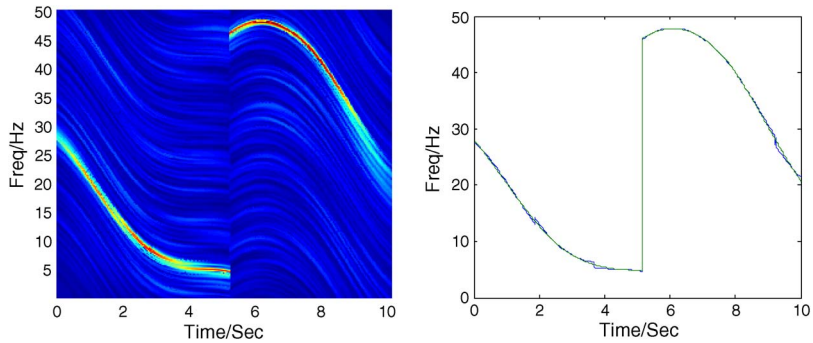

Fig. 3. SCT-based TFR and estimated IF in the second iteration.

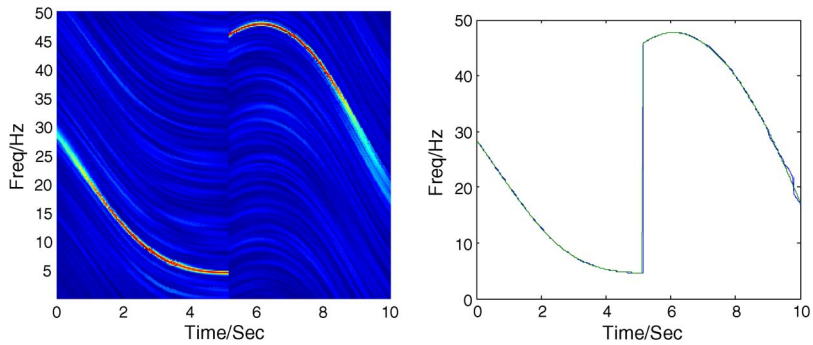

Fig. 4. SCT-based TFR and estimated IF in the third iteration.

In order to demonstrate the proposed parameter estimation method, an NLFM signal with piecewise IF denoted as follows is considered:

$$\Omega(t) = \begin{cases} 30 - 11t + 1.2t^2, & 0 \le t < 5s \\ -\frac{100}{3} + 26.5t - \frac{13}{6}t^2, & 5s \le t < 10s. \end{cases} \tag{17}$$

A Gaussian noise with a standard deviation of 0.6 and a mean of zero is artificially added to the signal. The SNR is thus 1.5468 dB. The window size is chosen as 512. δ is 0.015, and the sampling frequency is set to be 100 Hz. It takes six iterations before reaching the termination condition. The TFRs generated by the SCT and the estimated IFs in each iteration are shown in Figs. 2–7, respectively. The blue line denotes the estimated IF, and the red line denotes the approximated polynomial. The TFR generated by the SCT with initialized parameter $q = 0$ as illustrated in Fig. 2 is actually the result of the STFT. The energy of the signal is scattered along both the time and frequency axes, and it is unable to achieve an accurate estimation of the IF. A spline that is modified at the breaking point is used to approximate the estimated IF curve, as shown in Fig. 2. With the estimated parameters, the SCT improves the concentration of the TFR, and the extracted IF becomes closer to the true IF of the signal as shown in Figs. 3–6. The best TFR with a superior energy concentration and the precise estimation of the IF are shown in Fig. 7. The criterion of the termination condition is listed in Table I. In addition, in order to quantify the accuracy of the estimated IF compared to the true IF, the relative error is used to measure the difference between the estimated IF and the true IF. The relative error is defined as

$$error = mean\left(\int \frac{\left|\widetilde{\Omega}_{\text{iter}}(t) - \Omega(t)\right|}{|\Omega(t)|} dt\right). \tag{18}$$

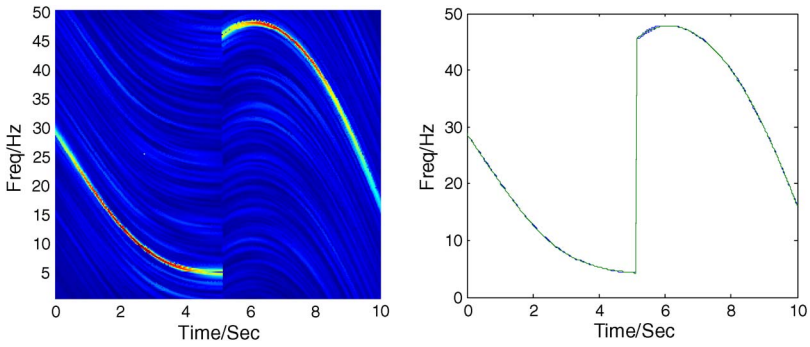

Fig. 5. SCT-based TFR and estimated IF in the fourth iteration.

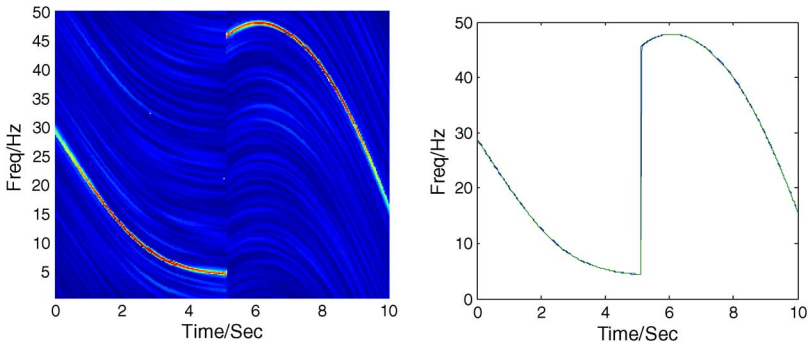

Fig. 6. SCT-based TFR and estimated IF in the fifth iteration.

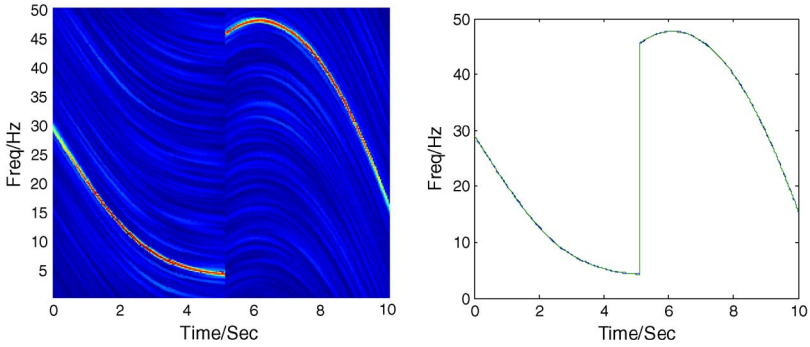

Fig. 7. SCT-based TFR and estimated IF in the sixth iteration.

TABLE I
VALUE OF THE TERMINATION CONDITION

Iteration	1	2	3	4	5
$\zeta(\%)$	7.424	2.723	1.988	1.544	1.482

TABLE II
ERRORS OF THE ESTIMATED IF

Iteration	1	2	3	4	5	6
Error (%)	9.270	4.182	2.736	2.437	2.050	1.964

Relative errors are listed in Table II, which clearly shows that the estimated IF is closer to the true IF in the proposed parameter estimation procedure.

IV. NUMERICAL STUDIES

In this section, three examples are used to demonstrate the effectiveness of the proposed SCT method. The first two examples are given in the form of $S(t) = \sin[2\pi\varphi(t)]$, whose IFs are given by

$$\Omega(t) = \frac{\partial\varphi(t)}{\partial t} = \frac{10(t-5)}{1+(t-5)^4} + 10, \quad (0 \le t \le 10s) \tag{19}$$

$$\Omega(t) = \frac{\partial\varphi(t)}{\partial t} = 10 + 2.5t + t^2/3 - t^3/40, \quad (0 \le t \le 18s). \tag{20}$$

Both of them are artificially added with additive Gaussian noise with a standard deviation of 0.6 and a mean of zero. The sampling frequency is set to be 100 Hz, and the window length is 512. The TFR obtained by the proposed SCT is compared with the TFRs obtained by conventional CT, continuous WT (CWT), and WVD. The parameters of the SCT are estimated using the proposed method presented in Section III.

The SNR of the first signal is 1.6482 dB. The TFRs generated by the CT, CWT, WVD, and SCT are shown in Fig. 8. The chirping rate of the CT is set to be 3.8 Hz/s. The TFR generated

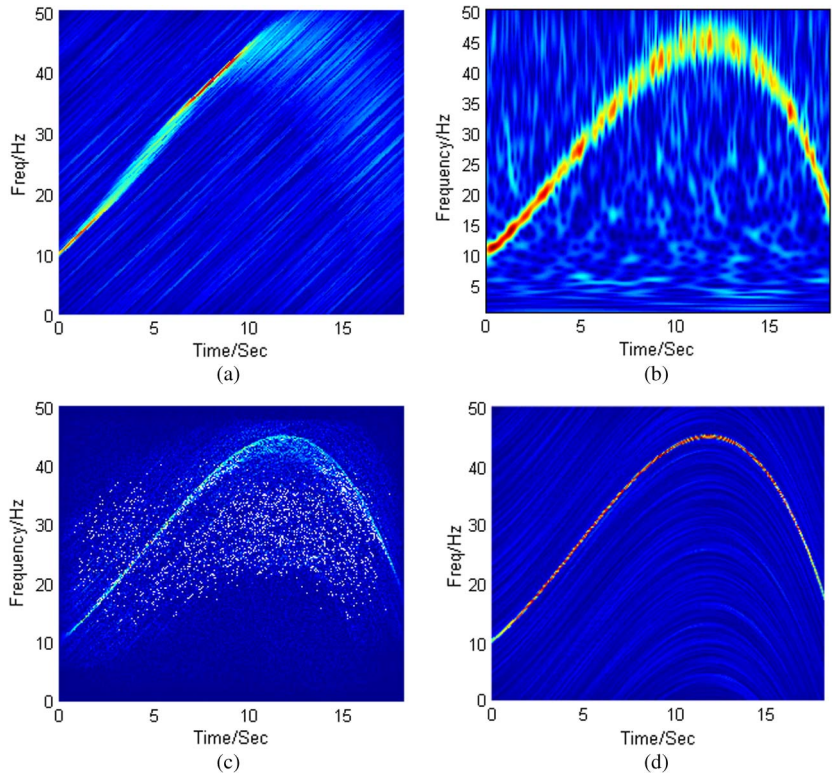

Fig. 8. TFR of the signal with IF in (20) by (a) CT, (b) CWT, (c) WVD, and (d) SCT.

TABLE III
PARAMETERS OF THE KERNEL OF THE SCT [FIG. 8(d)]

Piece	Coefficients			
(0,6)	`-0.025	0.333	2.500	10.000
(6,12)	-0.025	-0.117	3.800	31.600
(12,18)	-0.025	-0.567	-0.300	44.800

by the CT, shown in Fig. 8(a), can barely reveal the inherent time–frequency pattern of the signal. To be specific, the TFR only shows the clear IF trajectory over 0–10 s due to a good approximation by a linear function with a changing rate of 3.8 Hz/s. However, the TFR after 10 s is too blur to reveal the IF trajectory. In Fig. 8(b), it can be seen that the TFR generated by the CWT scatters the energy around the IF at the high-frequency region due to its coarse frequency resolution, and it is inaccurate to estimate the IF. As shown in Fig. 8(c), it is also difficult for the TFR generated by the WVD to differentiate the true IF trajectory from the spurious frequency contents introduced by the cross terms. On the other hand, as shown in Fig. 8(d), it is evident that the SCT outperforms the CT, the WT, and the WVD as it clearly reveals the true time–frequency pattern of the signal. The estimated coefficients of the SCT are listed in Table III.

The SNR of the second signal is 2.1159 dB. The TFRs generated by the CT, CWT, WVD, and the SCT are shown in Fig. 9. The chirping rate of the CT is set to be 9.5 Hz/s. As shown in Fig. 9(a), it is difficult for the TFR generated by the CT to identify the underlying time–frequency pattern of the signal since it is inadequate for the CT to analyze the NLFM signals. The TFR generated by the CWT, as shown in Fig. 9(b), shows poor time or frequency resolution because of the reciprocal relationship between the central frequency of the wavelet function and its window length. As shown in Fig. 9(c), the existence of spurious trajectories in the TFR obtained from the cross terms of the WVD strongly interferes the recognition of the true IF. However, in Fig. 9(d), the SCT provides the TFR with an excellent concentration, based on which the IF can be estimated precisely. The estimated coefficients of the SCT are listed in Table IV.

All of the tests are implemented by MATLAB version 7.11.0 (R2010b) on a PC with AMD Athlon 64 X2 dual-core processor $4000 + 2.10$ GHz and 1-GB RAM. The calculation times of the CT, the CWT, the WVD, and the one iteration of SCT with proper parameters for these two examples are listed in Table V. It can be seen that the calculation time of the SCT in one iteration is similar to that of the WVD in both cases, which is much less than that of CWT but slight more than that of CT.

In addition, a set of vibration signals collected by accelerometers on a rotor test rig during speed-up and shut-down processes is considered. The speed-up and shut-down processes of rotary machine usually contain valuable information related to the machine health condition, which plays an important role in machine condition monitoring. In this part, the SCT is used to implement the TFA for a set of the vibration signal collected during a speed-up and shut-down process. The test rig is shown in Fig. 10.

Fig. 11 shows the collected vibration signal. The sampling frequency is 100 Hz, and the window size is set to be 512. The spline kernel of order 4 with 18 pieces is adopted in the SCT. The termination condition in (16) is applied, and the threshold is set to be $\delta = 0.1\%$. Three iterations have been conducted before reaching the termination condition. Figs. 12

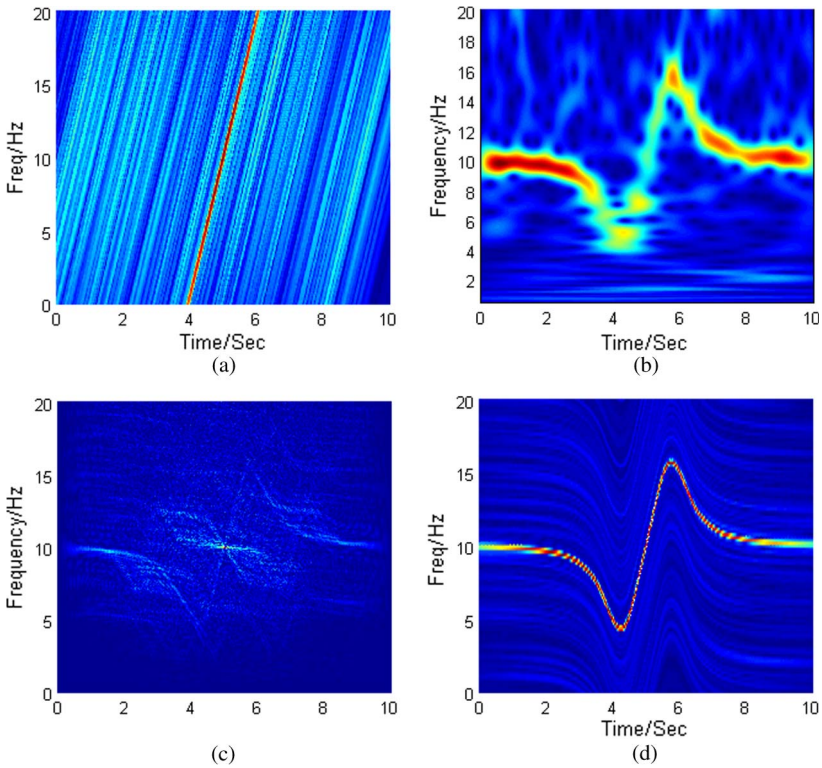

Fig. 9. TFR of signal with IF in (19) by (a) CT, (b) CWT, (c) WVD, and (d) SCT.

TABLE IV
PARAMETERS OF THE KERNEL OF THE SCT [FIG. 9(d)]

Piece	Coefficients			
(0,0.4)	-0.052	0.017	-0.055	9.920
(0.4,0.8)	0.018	-0.045	-0.066	9.898
(0.8,1.2)	-0.068	-0.024	-0.094	9.865
(1.2,1.6)	0.036	-0.106	-0.146	9.819
(1.6,2)	-0.228	-0.063	-0.213	9.746
(2,2.4)	0.091	-0.336	-0.373	9.636
(2.4,2.8)	-0.891	-0.227	-0.598	9.439
(2.8,3.2)	0.059	-1.296	-1.207	9.107
(3.2,3.6)	-3.227	-1.225	-2.215	8.420
(3.6,4)	8.946	-5.097	-4.744	7.132
(4,4.4)	9.064	5.639	-4.527	4.991
(4.4,4.8)	-15.566	16.516	4.335	4.663
(4.8,5.2)	3.606	-2.163	10.075	8.043
(5.2,5.6)	-15.566	2.163	10.075	11.957
(5.6,6)	9.064	-16.516	4.335	15.337
(6,6.4)	8.946	-5.639	-4.527	15.009
(6.4,6.8)	-3.227	5.097	-4.744	12.868
(6.8,7.2)	0.059	1.225	-2.215	11.580
(7.2,7.6)	-0.891	1.296	-1.207	10.893
(7.6,8)	0.091	0.227	-0.598	10.561
(8,8.4)	-0.228	0.336	-0.373	10.364
(8.4,8.8)	0.036	0.063	-0.213	10.254
(8.8,9.2)	-0.068	0.106	-0.146	10.181
(9.2,9.6)	0.018	0.024	-0.094	10.135
(9.6,10)	-0.052	0.045	-0.066	10.102

TABLE V
COMPARISON OF THE TIME COST

	CT	CWT	WVD	SCT(one iteration)
Signal in (34)	9.127 s	13.599 s	10.757 s	10.800 s
Signal in (35)	5.032 s	9.967 s	6.216 s	6.162 s

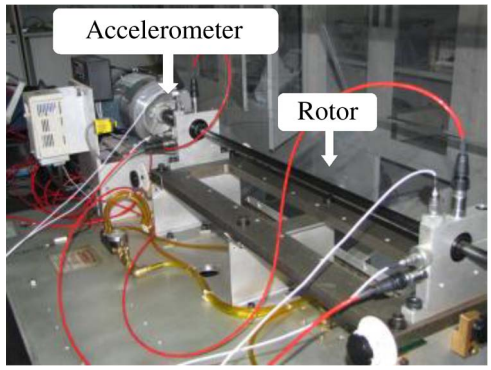

Fig. 10. Rotor test rig.

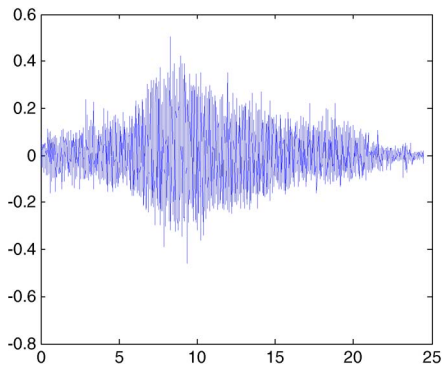

Fig. 11. Set of vibration signal.

and 13 show the TFRs and the estimated instantaneous speed obtained by the STFT and the SCT, respectively. It is clear that the TFR shown in Fig. 13 has much better energy concentration

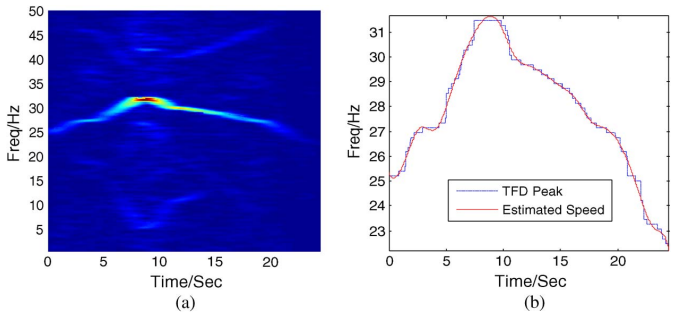

Fig. 12. TFR generated by (a) the STFT and (b) the extracted ridge and the estimated instantaneous rotating speed.

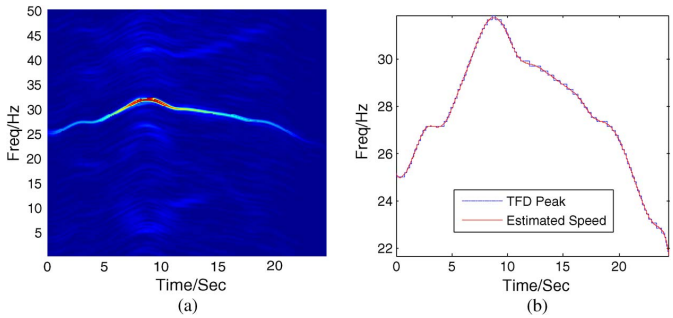

Fig. 13. TFR generated by (a) the SCT and (b) the extracted ridge and the estimated instantaneous rotating speed.

TABLE VI
PARAMETERS OF TRANSFORM KERNEL OF THE SCT (FIG. 13)

Piece	Coefficients			
(0,1.37)	-0.221	1.141	-0.717	25.101
(1.37,2.73)	-0.244	0.237	1.158	25.680
(2.73,4.09)	0.353	-0.761	0.446	27.079
(4.09,5.45)	-0.180	0.682	0.339	27.168
(5.45,6.81)	0.037	-0.051	1.199	28.440
(6.81,8.17)	-0.158	0.099	1.264	30.070
(8.17,9.53)	0.009	-0.546	0.655	31.573
(9.53,10.89)	0.263	-0.511	-0.783	31.475
(10.89,12.25)	-0.175	0.565	-0.709	30.128
(12.25,13.62)	0.036	-0.149	-0.143	29.768
(13.62,14.98)	0.007	-0.002	-0.349	29.387
(14.98,16.34)	-0.062	0.027	-0.315	28.926
(16.34,17.7)	0.144	-0.226	-0.586	29.391
(17.7,19.06)	-0.174	0.360	-0.404	27.536
(19.06,20.42)	0.033	-0.349	-0.389	27.216
(20.42,21.78)	0.083	-0.215	-1.156	26.124
(21.78,23.14)	0.089	0.123	-1.281	24.361
(23.14,24.5)	-0.726	0.487	-0.451	23.070

for the fundamental frequency component than that of TFR given in Fig. 12. This indicated that the SCT is able to achieve more accurate estimation of the instantaneous speed of the rotor undergoing the speed-up and shut-down processes than the STFT. The instantaneous rotating speed is represented in ppform, and the parameters of the transform kernel of the SCT q_k^i, for all i and k, are listed in Table VI.

It is worth noticing that the proposed SCT is focused on monocomponent signals. For the multicomponent signals with multiple-frequency components which need to be approximated with different spline functions, the SCT is not applicable. It is a common problem for parameterized time–frequency transforms. Using the vibration signals collected from the rotor test rig as an example, the energy at the frequency components other than the fundamental frequency component in the TFR generated by the SCT is more scattered than that of the TFR generated by STFT. The authors are currently working on extending the SCT to the signals containing multiple-frequency components.

V. CONCLUSION

The conventional time–frequency transform methods cannot characterize the accurate time–frequency patterns for the signals with time-varying frequency due to the poor energy concentration. A novel time–frequency transform has been proposed to characterize the underlying time–frequency feature of the signal with nonlinearly time-varying IF trajectory. With the effective algorithm developed to estimate the parameters of transform kernel of the SCT, its potential and effectiveness are validated through analyzing several numerical simulation signals and a set of experimental vibration signals. The comparison results show that the SCT outperforms the STFT, the CWT, the conventional CT, and the WVD in providing the TFR of better energy concentration and achieving more accurate IF estimation for the signals with nonlinearly time-varying IF. Future work will focus on extending the SCT from monocomponent signal analysis to multicomponent signal analysis.

REFERENCES

[1] B. Boashash, "Estimating and interpreting the instantaneous frequency of a signal-Part I: Fundamentals," *Proc. IEEE*, vol. 80, no. 4, pp. 520–538, Apr. 1992.
[2] B. Boashash, "Estimating and interpreting the instantaneous frequency of a signal-Part II: Algorithms and applications," *Proc. IEEE*, vol. 80, no. 4, pp. 540–568, Apr. 1992.
[3] M. Blodt, D. Bonacci, J. Regnier, M. Chabert, and J. Faucher, "On-line monitoring of mechanical faults in variable-speed induction motor drives using the Wigner distribution," *IEEE Trans. Ind. Electron.*, vol. 55, no. 2, pp. 522–533, Feb. 2008.
[4] E. Strangas, S. Aviyente, and S. Zaidi, "Time–frequency analysis for efficient fault diagnosis and failure prognosis for interior permanent-magnet AC motors," *IEEE Trans. Ind. Electron.*, vol. 55, no. 12, pp. 4191–4199, Dec. 2008.
[5] J. A. Rosero, L. Romeral, J. A. Ortega, and E. Rosero, "Short-circuit detection by means of empirical mode decomposition and Wigner–Ville distribution for PMSM running under dynamic condition," *IEEE Trans. Ind. Electron.*, vol. 56, no. 11, pp. 4534–4547, Nov. 2009.
[6] M. Pineda-Sanchez, M. Riera-Gausp, J. Roger-Folch, J. A. Antonino-Daviu, J. Perez-Cruz, and R. Puche-Panadero, "Diagnosis of induction motor faults in time-varying conditions using the polynomial-phase transform of the current," *IEEE Trans. Ind. Electron.*, vol. 58, no. 4, pp. 1428–1439, Apr. 2011.
[7] A. Stefani, A. Bellini, and F. Filippetti, "Diagnosis of induction machines' rotor faults in time-varying conditions," *IEEE Trans. Ind. Electron.*, vol. 56, no. 11, pp. 4548–4556, Nov. 2009.
[8] J. Rosero, J. Cusido, A. G. Espinosa, J. A. Ortega, and L. Romeral, "Broken bearings fault detection for a permanent magnet synchronous motor under non-constant working conditions by means of a joint time frequency analysis," in *Proc. IEEE Inter. Symp. Ind. Electron.*, Vigo, Spain, 2007, pp. 3415–3419.
[9] H. C. Lin, "Fast tracking of time-varying power system frequency and harmonics using iterative-loop approaching algorithm," *IEEE Trans. Ind. Electron.*, vol. 54, no. 2, pp. 974–983, Apr. 2007.
[10] L. Coppola, Q. Liu, S. Buso, D. Boroyevich, and A. Bell, "Wavelet transform as an alternative to the short-time Fourier transform for the study of conducted noise in power electronics," *IEEE Trans. Ind. Electron.*, vol. 55, no. 2, pp. 880–887, Feb. 2008.
[11] J. J. Silva, K. M. Silva, A. Lima, and J. Neto, "Fouling detection based on analysis of ultrasonic guided waves using wavelet transform," in *Proc. IEEE Int. Symp. Ind. Electron.*, Cambridge, U.K., 2008, pp. 1187–1191.

[12] N. Derakhshan and M. H. Savoji, "Perceptual speech enhancement using Hilbert transform," in *Proc. IEEE Inter. Symp. Ind. Electron.*, Montreal, QC, Canada, 2007, pp. 681–684.
[13] W. X. Yang, P. J. Tavner, C. J. Crabtree, and M. Wilkinson, "Cost-effective condition monitoring for wind turbines," *IEEE Trans. Ind. Electron.*, vol. 57, no. 1, pp. 263–271, Jan. 2009.
[14] Z. Leonowicz and T. Lobos, "Analysis of traction system time-varying signals using ESPRIT subspace spectrum estimation method," in *Proc. Conf. IEEE Ind. Electron.*, Paris, France, 2007, pp. 3424–3427.
[15] L. Cohen, "Time–frequency distributions-a review," *Proc. IEEE*, vol. 77, no. 7, pp. 941–981, Jul. 1989.
[16] L. Cohen, *Time–Frequency Analysis*. Upper Saddle River: Prentice-Hall, 1995, pt. 2, pp. 30–52.
[17] S. H. Nawab and T. F. Quatieri, *Short-Time Fourier Transform*. Upper Saddle River, NJ: Prentice-Hall, 1987.
[18] H. K. Kwok and D. L. Jones, "Improved instantaneous frequency estimation using an adaptive short-time Fourier transform," *IEEE Trans. Signal Process.*, vol. 48, no. 10, pp. 2964–2972, Oct. 2000.
[19] P. J. Kootsookos, B. C. Lovell, and B. Boashash, "A unified approach to the STFT, TFDs, and instantaneous frequency," *IEEE Trans. Signal Process.*, vol. 40, no. 8, pp. 1971–1982, Aug. 2002.
[20] A. Bouzida, O. Touhami, R. Ibtiouen, M. Fadel, A. Rezzoug, and A. Beloucherani, "Fault diagnosis in industrial induction machines through discrete wavelet transform," *IEEE Trans. Ind. Electron.*, vol. 58, no. 9, pp. 4385–4395, Sep. 2011.
[21] F. Hlawatsch and G. F. Boudreaux-Bartels, "Linear and quadratic time–frequency signal representations," *IEEE Signal Process. Mag.*, vol. 9, no. 2, pp. 21–67, Apr. 1992.
[22] G. Kaiser, *A Friendly Guide to Wavelets (Modern Birkhäuser Classics)*. Cambridge, MA: Birkhäuser Boston, 2011, pt. 1, pp. 60–77.
[23] S. Mann and S. Haykin, "The chirplet transform: Physical considerations," *IEEE Trans. Signal Process.*, vol. 43, no. 11, pp. 2745–2761, Nov. 1995.
[24] D. Mihovilovič and R. N. Bracewell, "Whistler analysis in the time–frequency plane using chirplets," *J. Geophys. Res.*, vol. 97, no. A11, pp. 17 199–17 204, Nov. 1992.
[25] E. Chassande-Mottin and A. Pai, "Best chirplet chain: Near-optimal detection of gravitational wave chirps," *Phys. Rev. D*, vol. 73, no. 4, pp. 42 003–42 026, Feb. 2006.
[26] D. Mihovilovic and R. N. Bracewell, "Adaptive chirplet representation of signals on time–frequency plane," *Electron. Lett.*, vol. 27, no. 13, pp. 1159–1161, Jun. 1991.
[27] J. Cui and W. Wong, "The adaptive chirplet transform and visual evoked potentials," *IEEE Trans. Biomed. Eng.*, vol. 53, no. 7, pp. 1378–1384, Jul. 2006.
[28] S. Mann and S. Haykin, ""Chirplets" and "warblets": Novel time–frequency methods," *Electron. Lett.*, vol. 28, no. 2, pp. 114–116, Jan. 1992.
[29] B. Boashash, *Time Frequency Signal Analysis and Processing: A Comprehensive Reference*. Amsterdam, The Netherlands: Elsevier, 2003, pt. 4, pp. 229–368.
[30] G. L. Xu, X. T. Wang, and X. G. Xu, "Time-varying frequency-shifting signal assisted empirical mode decomposition method for AM–FM signals," *Mech. Syst. Signal Process.*, vol. 23, no. 8, pp. 2458–2469, Nov. 2009.
[31] [Online]. Available: http://mathworld.wolfram.com/WeierstrassApproximationTheorem.html
[32] C. De Boor, *A Practical Guide to Splines*. New York: Springer-Verlag, 2001, pt. 7, pp. 17–20.
[33] J. H. Ahlberg, E. N. Nilson, and J. L. Walsh, *The Theory of Splines and Their Applications*. New York: Academic, 1967, pt. 1, pp. 1–8.
[34] M. Unser, A. Aldroubi, and M. Eden, "B-spline signal processing. I. Theory," *IEEE Trans. Signal Process.*, vol. 41, no. 2, pp. 821–833, Feb. 1993.
[35] M. Unser, A. Aldroubi, and M. Eden, "B-spline signal processing. II. Efficiency design and applications," *IEEE Trans. Signal Process.*, vol. 41, no. 2, pp. 834–848, Feb. 1993.
[36] D. Lasser and J. Hoschek, *Fundamentals of Computer Aided Geometric Design*. New York: Elsevier, 2002.

Y. Yang received the B.S. and M.S. degrees in mechanical engineering from Shanghai Jiao Tong University, Shanghai, China, in 2006 and 2009, respectively, where she is currently working toward the Ph.D. degree in the Mechanical Engineering Department. She studied at the Intelligent Maintenance System Center, University of Cincinnati, Cincinnati, OH, from 2007 to 2008.

She is currently with the State Key Laboratory of Mechanical System and Vibration, Shanghai Jiao Tong University. Her research interests include signal processing, machine health diagnosis, and prognostics.

Z. K. Peng received the B.Sc. and Ph.D. degrees from Tsinghua University, Beijing, China, in 1998 and 2002, respectively.

From 2003 to 2004, he was with the City University of Hong Kong, Kowloon, Hong Kong, as a Research Associate, and then, he was with Cranfield University, Cranfield, U.K., as a Research Officer. After that, he was with the University of Sheffield, Sheffield, U.K., for four years. He is currently a Research Professor with the State Key Laboratory of Mechanical System and Vibration, Shanghai Jiao Tong University, Shanghai, China. His main expertise relates to the subject areas of nonlinear vibration, signal processing and condition monitoring, and fault diagnosis for machines and structures.

G. Meng received the Ph.D. degree from Northwestern Polytechnical University, Xi'an, China, in 1988.

In 1993, he was a Professor and the Director of Vibration Engineering Institute with Northwestern Polytechnical University. From 1989 to 1993, he was also a Research Assistant with Texas A&M University, College Station, an Alexander von Humboldt Fellow with Technical University Berlin, Berlin, Germany, and a Research Fellow with New South Wales University, Sydney, Australia. From 2000 to 2008, he was with Shanghai Jiao Tong University, Shanghai, China, as the Cheung Kong Chair Professor, the Associate Dean, and the Dean of the School of Mechanical Engineering. He is currently a Professor and the Director of the State Key Laboratory of Mechanical System and Vibration, Shanghai Jiao Tong University. His research interests include dynamics and vibration control of mechanical systems, nonlinear vibration, and microelectromechanical systems.

W. M. Zhang was born in May 1978. He received the B.S. degree in mechanical engineering and the M.S. degree in mechanical design and theories from Southern Yangtze University, Wuxi, China, in 2000 and 2003, respectively, and the Ph.D. degree in mechanical engineering from Shanghai Jiao Tong University, Shanghai, China, in 2006.

He is currently an Associate Professor with the State Key Laboratory of Mechanical System and Vibration, School of Mechanical Engineering, Shanghai Jiao Tong University. He has deep experiences in the dynamics and control for micro-/nanoelectromechanical systems (MEMS/NEMS). His researches involve nonlinear dynamics and chaos control, nonlinear vibration and control, coupled parametrically excited microresonators, and the reliability analysis and assessment for MEMS/NEMS applications.